

Experimental capacity of perforated cold-formed steel open sections under compression and bending

Maurizio Orlando ^{*1}, Giovanni Lavacchini ^{2a}, Barbara Ortolani ^{3b} and Paolo Spinelli ^{1c}

¹ Department of Civil and Environmental Engineering, University of Florence, Via di S. Marta 3, 50139 Florence, Italy

² Studio Giovanni Lavacchini, Via IV Novembre 46/3, 50032 Borgo San Lorenzo (FI), Italy

³ Via dell'Arcoiaio 52, 50137 Florence, Italy

(Received October 04, 2016, Revised March 03, 2017, Accepted March 21, 2017)

Abstract. This study evaluates the reliability of present European codes in predicting the collapse load of columns made with perforated cold-formed steel (CFS) profiles under combined axial load and bending. To this aim, a series of experimental tests on slender open-section specimens have been performed at varying load eccentricity. Preliminarily, stub column tests have also been performed to calculate the effective section properties of the investigated profile. By comparison of experimental data with code-specified M-N strength domains, the authors demonstrate that present code formulations may underestimate the collapse load of thin-walled perforated open sections. The study is the first step of a wider experimental and numerical study aimed at better describing strength domains of perforated CFS open sections.

Keywords: industrial pallet racks; cold-formed steel; experimental tests; M-N strength domain; Eurocode 3

1. Introduction

A large amount of the steel production in the world concerns cold-formed steel (CFS) open sections, most of which belong to class 4 cross-sections according to EN 1993-1-1 (CEN 2006a). These profiles often fail due to local buckling before the steel yields. CFS sections are made by rolling or pressing thin gauges of steel sheets, and may be used for special structural members or for a complete bearing system. The use of these profiles is more competitive than hot rolled profiles in some types of structures, like industrial steel storage pallet racks (Bernuzzi and Castiglioni 2001, Ungureanu *et al.* 2016), and in the structural upgrade of existing reinforced concrete structures (Foraboschi 2016).

Usually CFS storage rack columns are provided with a regular series of holes along the whole length, and their section has only one axis of symmetry. Holes are needed for making dry connections between beams and uprights at different levels, but they require special attention from a design point of view. If on one side these structural assemblies present some advantages like lightness, large variety of shapes and low costs, on the other side they are buckling-sensitive structures.

CFS uprights with open section, subjected to centric or eccentric axial load, may buckle in three different modes, or a combination of them (Fig. 1) (Schafer 2002, Silvestre and

Camotim 2003): local, distortional or global buckling, where the last mode can be classified as flexural, torsional or flexural-torsional. Each buckling mode is characterized by a different post-buckling strength and a different collapse shape.

Local buckling is characterized by the deformation of the component plate elements of the section (Fig. 1(a)). Distortional buckling, also known as “stiffener buckling” or “local-torsional buckling”, occurs with the rotation of the flange at the flange/web junction in members with edge stiffened elements, and with the displacement of the intermediate stiffener normal to the plane of the element (Fig. 1(b)) in members with intermediate stiffeners. Global buckling affects the beam along its whole length, without distortion of the section (Fig. 1(c)), and it can be classified into: flexural buckling (Fig. 1(c(i))) if the transversal section bends about one of the principal inertial axes, torsional buckling (Fig. 1(c(ii))) if the transversal section twists about the shear center, and flexural-torsional buckling (Fig. 1(c(iii))) if a combination of flexural and torsional buckling arises.

A common design procedure to evaluate the section strength of slender sections utilizes the concept of effective width, based on the work of Kàrmàn *et al.* (1932). They early studied the complex non-uniform distribution of stresses in a thin buckled plate under compression and observed that local buckling of a plate element causes a concentration of longitudinal stresses near its supporting edges, so they introduced the concept of equivalent or effective width (b_e) to evaluate the collapse load of the plate. The cross-section is divided into plane elements, whose width and thickness are denoted by b and t , respectively. If the generic element $b \times t$ is subjected to a uniform compression in one of the principal directions, it

*Corresponding author, Ph.D., Associate Professor,
E-mail: maurizio.orlando@unifi.it

^a Civil Engineer

^b Ph.D., Civil Engineer

^c Full Professor

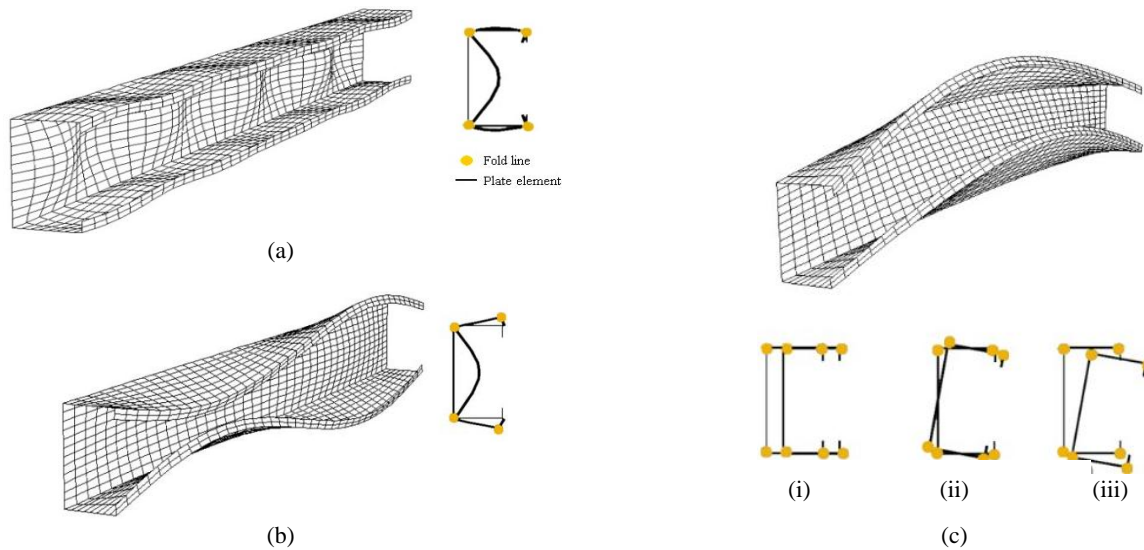


Fig. 1 Buckling modes: (a) local buckling; (b) distortional buckling; (c) global buckling (Silvestre and Camotim 2003)

collapses under a non-uniform distribution of stresses, with maximum values at the corners and minimum values in the fibers far away from corners. The effective width b_{eff} is defined as the width of an equivalent plate collapsing under a uniform distribution of stresses, whose intensity equals the maximum value in the actual non uniform distribution.

Von Karman's method neglects geometrical imperfections, which on the contrary influence significantly the structural response, especially in the post-buckling field. Later Winter improved Von Karman's formulation for the evaluation of the effective width, introducing the influence of geometrical imperfections. Winter's equation is internationally accepted for the evaluation of the compressive strength taking into account effects of local buckling for CFS profiles; it is included in all documents dealing with the design of cold formed steel structures. The "effective width" method is the most used for evaluating the local buckling load of CFS profiles (CEN 2006b and c). Nevertheless, the most general methods for dealing with buckling of CFS open sections are the Finite Element Method (FEM) (Sivakumaran and Abdel-Rahman 1998, Davies 2000, Lian *et al.* 2016), the Finite Strip Method (FSM) (Papangelis and Hancock 1995, Davies 2000, Li and Schafer 2010), or the Generalized Beam Theory (GBT) (Kesti and Davies 1999, Rondal 2000, Camotim *et al.* 2010). Although these methods are the most efficient and the most utilized for the evaluation of the critical buckling load, each of them has some limitations. Finite element models allow buckling modes of every type of structural element, under different load and restraint conditions, to be investigated, but they do not differentiate buckling modes automatically, so the user has to classify them through a visual analysis of the buckling configuration. The FSM allows for evaluating automatically the critical load as a function of the effective length. This method helps the user in identifying buckling modes, as in many cases the first minimum point of the curve identifies local buckling and the second minimum point is often associated with distortional buckling.

Nevertheless, the FSM is limited in its applicability to prismatic elements without holes and with simple restraint

conditions. Finally, the GBT allows for automatically classifying buckling modes and getting the critical stress. This method introduces some simplifications, which make it advantageous for regular geometric configurations, boundary conditions and applied loads.

For CFS elements with holes along their length additional problems arise in the evaluation of the buckling load. For these elements the Equivalent Thickness Method (Szabo and Dubina 2004, Salhab and Wang 2008) may be used, where CFS plates with holes are approximated to continuous walls with a reduced thickness having the same total volume; this method works well only for small holes. Other analytical solutions for CFS elements with holes have been proposed in literature: e.g., Moen and Schafer (2009) developed approximate expressions assuming that the critical elastic buckling stress is controlled either by buckling of the unstiffened strip adjacent to the hole, or by plate buckling away from a hole.

For uprights of industrial pallet racks, besides the presence of holes, geometrical imperfections play a key role (Crisan *et al.* 2012a, b, Ungureanu *et al.* 2016, Zagari *et al.* 2016), so experimental tests are required for reliably evaluating buckling loads, similarly to columns made of other materials, like reinforced concrete (Angotti *et al.* 2002) or glass (Foraboschi 2014). Literature experimental tests on perforated CFS beams may be classified in: tests to check the reliability of analytical predictive methods and/or code design rules (Davies *et al.* 1997, Sivakumaran and Abdel-Rahman 1998, Kesti and Davies 1999, Yan and Young 2002, Young and Chen 2008, Lavacchini *et al.* 2013); tests to investigate the influence of holes on the strength (Bernuzzi and Castiglioni 2001, Lecce and Rasmussen 2006a, b); tests to investigate the influence of the hole shape (rectangular, oval, etc.) (Sivakumaran and Abdel-Rahman 1998) or restraint conditions (Young and Rasmussen 1998, Kesti and Davies 1999, Sarawit and Pekoz 2001, Teh *et al.* 2004, Craveiro *et al.* 2016).

In this paper, the authors illustrate results of an experimental campaign on CFS perforated storage rack columns under centric or eccentric axial load at varying

eccentricity. The work is part of a wider research program (StruMetal 2015), aimed at investigating the load-carrying capacity and the seismic response of steel pallet racks. Experimental results are compared with European code-specified $M-N$ domains, specifically with formulations given in EN 1993-1-1 (CEN 2006a) and EN 15512 (CEN 2009). The main objective of the work is to test the reliability of these formulations for the design of CFS structures, although limited to a particular distribution of bending moments, and to collect data for the calibration of a numerical FE model, which will be used to extend the study to other bending distributions and other CFS open sections. The nonlinear finite element model has already been calibrated on experimental results and numerical nonlinear simulations will be performed to investigate the structural response of the investigated section for additional values of the eccentricity, in one or two directions, as during the experimental campaign only a limited number of positions of the pressure center were considered. Numerical analyses will be performed taking into account both geometrical and mechanical nonlinearities, and a high number of eccentricities and directions, so a better approximation of the strength domain of the investigated profile could be obtained. Finite element analyses will also be used to evaluate the capacity of the same CFS open section subjected to a uniform distribution of bending moments, as the testing machine allows for applying an eccentric load only at one end (triangular diagram of the bending moment). The aim is to eliminate approximations introduced in the construction of code-specified $M-N$ curves when equivalent uniform bending moment coefficients are adopted, as well as the authors made in this work to bring back the triangular shape of the bending moment diagram adopted in “member buckling” tests to an equivalent uniform bending moment. Results will be presented in a forthcoming paper (Bertocci *et al.* 2016).

2. Experimental setup

For CFS columns made with open profiles, and having holes regularly distributed along the length, experimental tests are the only reliable tool to evaluate the structural behavior. Although many studies have been performed on the effect of holes on the strength of these profiles, a general analytical solution is not available, therefore present codes recommend evaluating the load bearing of CFS perforated columns through experimental tests (CEN 2009).

The authors performed an experimental campaign on CFS columns with the same open profile and two different lengths; specimens were subjected to centric or eccentric axial load at varying eccentricity with symmetrical or unsymmetrical bending. The length of specimens was chosen to investigate both local and distortional buckling modes. Ten stub-column tests were performed to investigate local buckling; 27 “member buckling” tests were performed to investigate global and distortional buckling.

2.1 Specimens

Tests were performed on CFS specimens with an open

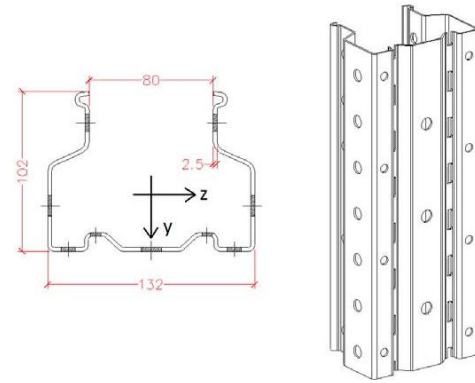


Fig. 2 Profile used in the experimental campaign (dimensions in mm)

Table 1 Mechanical properties of S350GD steel

Elasticity modulus E	N/mm ²	210,000
Poisson ratio ν	-	0.3
Shear modulus G	N/mm ²	80,769
Specific weight γ_s	kN/m ³	78.5
Characteristic yield strength f_{yk}	N/mm ²	350
Characteristic ultimate strength f_u	N/mm ²	420

profile (Fig. 2) produced by the Italian company ROSS S.p.A. and made of S350GD steel (Table 1). Two specimen lengths were considered: 450 mm for stub-column tests and 1020 mm for “member buckling” tests. Table 2 lists geometrical dimensions and inertial properties of the chosen profile. All specimens were taken from the current production of the company, cutting some elements into the desired lengths.

2.2 Experimental equipment

The experimental equipment was formed by (Fig. 3):

- a steel frame;
- a hydraulic jack to apply the load to the specimen; the jack was fixed to the upper crossbeam of the frame and connected to an oleodynamic pump;
- a load cell positioned on the lower crossbeam of the frame;
- two linear variable displacement transducers (LVDT) to record the vertical displacements of the specimen's upper end on both sides of the bending plane;
- an electronic control unit, to which the load cell and LVDT were connected;
- a PC connected to the control unit through an ad-hoc software.

A steel rectangular plate was inserted on both the lower part of the hydraulic jack and the upper part of the load cell, to distribute uniformly the applied load.

Specimens were equipped at both ends with a couple of housing plates, to allow specimens to be installed in the testing machine. Each couple was formed by two 15 mm

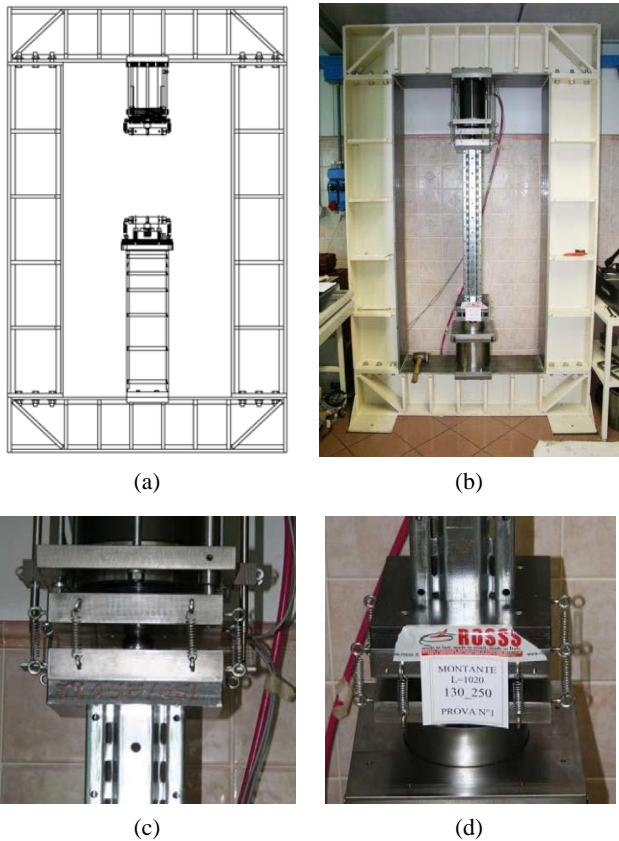


Fig. 3 Test setup: (a) frontal view; and (b) picture of the testing machine; (c) loading plates at the specimen's



Fig. 4 Housing plates: (a) holes for bolts connecting the two plates of each couple; (b) hole with the profile perimeter in the upper plate; (c) inner plate to block section against inward distortion

thick steel plates, hold together by four bolts. The plate fixed to the specimen had a central hole, whose perimeter followed the outer perimeter of the specimen's profile (Fig. 4(a)). Each specimen's end was inserted inside the hole and

Table 2 Properties of the CFS profile used for specimens

Gross area of cross-section A_{gr}	mm ²	982
Net area of cross-section (without holes) A_{net}	mm ²	816
Moment of inertia about the strong axis y $J_{y,gr}$	mm ⁴	2,362,919
Moment of inertia about the weak axis z $J_{z,gr}$	mm ⁴	1,120,111
Radius of gyration about y -axis $\rho_{y,gr}$	mm	49.05
Radius of gyration about z -axis	mm	33.77



Fig. 5 Specimen ready for a stub-column test

blocked against inward distortion through the insertion of an inner plate (Fig. 4(b)); the restraint was unilateral, able to transmit only compressive stresses, so in case the center of pressure was out of the central core of inertia, the specimen's end could detach from the plate on the tensile part. Fig. 5 shows one of the specimens used for stub-column tests, equipped with housing plates at both ends.

In tests under eccentric axial load, the load eccentricity was only applied at the base of the specimen by changing the position of the load cell, so a triangular distribution of bending moments was applied to specimens. The distribution of bending moments was chosen to reproduce the typical stress state present on half height of storage rack columns under vertical loads.

Finally, a spherical hinge was put between each couple of plates and the plates fixed to the testing machine, to allow specimen's ends to rotate about any axis.

3. Experimental campaign

Tests were performed under load control, and consisted of following steps:

- pre-loading of the specimen up to about 5% of the estimated collapse load and successive unloading;
- loading of the specimen up to the maximum load;
- unloading up to separate the specimen's upper end from the testing machine.

Preliminarily, with the aim of evaluating the effective properties of the cross-section, ten stub-column specimens were subjected to centric axial load. Their dimensions were

chosen to satisfy geometrical limits suggested in EN 15512 (CEN 2009). The experimental effective area of the profile was found to be equal to 83% of the gross area (Table 2).

To investigate distortional and global buckling modes, 27 tests were performed on 1020 mm long specimens. These specimens were subjected to centric or eccentric axial load, with increasing values of the eccentricity with symmetrical or unsymmetrical bending.

3.1 Combined compression and uniaxial bending about the strong axis y

Following tests were performed (Fig. 6):

- three specimens were loaded under centric axial load (tests no. 1÷3);
- three specimens were loaded under eccentric load with symmetrical bending about the strong axis y; the value of the eccentricity at the specimen's lower end was equal to 18 mm, which corresponds to half the radius of the central core of inertia (tests no. 4÷6); as in test no. 5 the specimen exhibited a buckling shape different than the other two tests, an additional test (test no. 7) was performed, where the specimen buckled similarly to specimens no. 4 and 6;

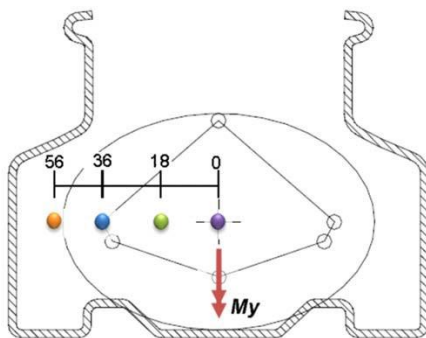


Fig. 6 Positions of the center of pressure in tests with bending about the strong axis y

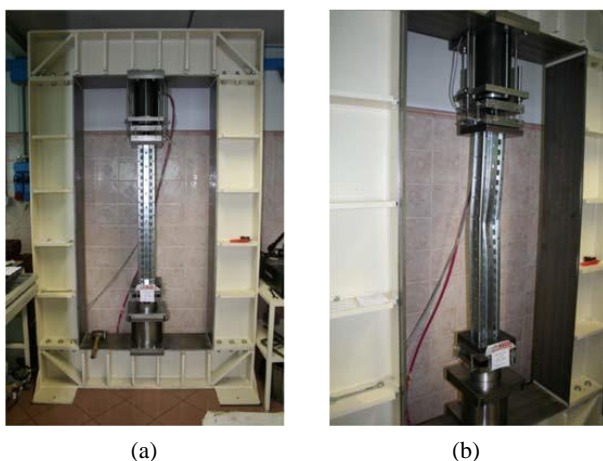


Fig. 7 Pictures of a “member buckling” test: (a) undeformed specimen; (b) buckled specimen at the end of the test

- three specimens were loaded with an eccentricity value of 36 mm, which is equal to the radius of the central core of inertia (tests no. 8÷10);
- seven specimens were loaded with an eccentricity value of 56 mm, which is equal to 1.5 times the radius of the central core of inertia (tests no. 11÷17).

In each “member buckling” test, the ultimate load of the specimen was determined and the buckling mode was identified (Fig. 7).

Table 3 lists results of tests and compare them with maximum loads given by EN1993-1-1 (CEN 2006a).

From experimental results with bending about y axis, following conclusions can be drawn:

- all specimens loaded with the same eccentricity e_z exhibited about the same experimental collapse load, except for four specimens (tests no. 5, 8, 16 and 17), which collapsed under a higher load than other specimens (Table 3) due to likely lower imperfections in specimens no. 5 and 8, and to a slight modification of the restraint device at the specimen's lower base in tests no. 16 and 17;
- the collapse load decreases as the eccentricity increases, for $e_z = 56$ mm it is about half the collapse load under centric axial load;
- all specimens loaded under eccentric axial load exhibited a global buckling mode, which was accompanied by distortional buckling in tests with $e_z = 36$ mm and local buckling in tests with $e_z = 56$ mm.

3.2 Combined compression and uniaxial bending about the weak axis z

Three specimens were loaded under eccentric axial load with symmetrical bending about the weak axis z (tests no. 18÷20); the eccentricity at the specimen's lower end was chosen equal to $e_y = 18$ mm, which is equal to the radius of the central core of inertia along the y axis on the web side (Fig. 8). Fig. 9 shows one of these specimens after the local buckling collapse, while Table 4 lists results of all the three tests.

Main results of tests with bending about the weak axis z are:

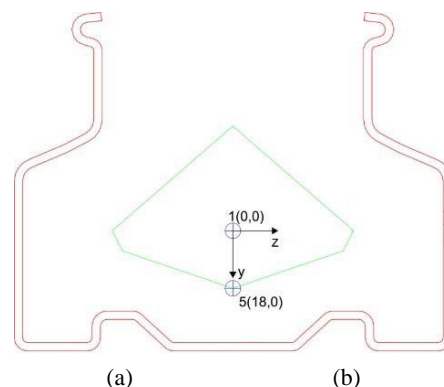


Fig. 8 Positions of the load application point with eccentricity e_y about the weak axis z

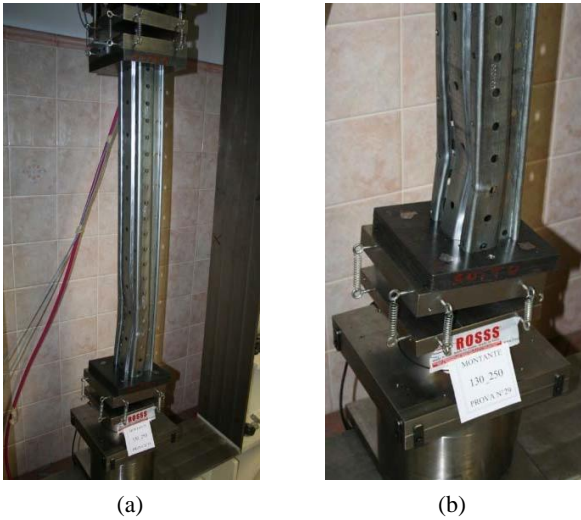


Fig. 9 Pictures at the end of test no. 18: (a) global view; (b) detail of the specimen's lower end

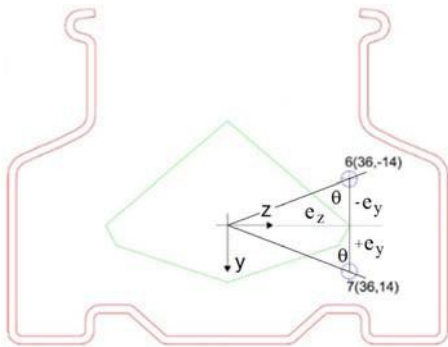


Fig. 10 Positions of the center of pressure in tests with bending about the weak axis z

- the collapse load has about the same value of specimens loaded with the same eccentricity of 18 mm about the strong axis y ;
- on average, the collapse load is underestimated of more than 30% by EN1993-1-1;
- all three specimens exhibited a local buckling mode.

3.3 Combined compression and biaxial bending

Finally, some tests were performed under axial load and unsymmetrical bending, which is the typical stress condition of storage rack uprights during an earthquake. Vertical loads combined with seismic horizontal loads induce axial load combined with bending about both axes y and z .

As the profile is not symmetrical about the weak axis z , it was required to perform twice the test for each value of the eccentricity e_y in the y -direction. Seven tests under combined compression and biaxial bending were performed (Table 5):

- three tests (tests no. 21÷23) with $e_z = 36$ mm and $e_y = -14$ mm (point no. 6 in Fig. 10), which are equal, respectively, to the radius of the central core of inertia and to the maximum transversal eccentricity allowed by the testing machine;
- four tests (tests no. 24÷27) with $e_z = 36$ mm and $e_y = 14$ mm (point no. 7 in Fig. 10).

Tests with unsymmetrical bending showed that:

- all specimens collapsed at about the same load, even if three tests with negative values of e_y and four tests were conducted for positive values of e_y ;
- on average, the collapse load is underestimated of more than 30% by EN1993-1-1;

Table 4 Results of tests under eccentric load with bending about the weak axis z

ID	Eccentricity e_z (mm)	Buckling mode ⁽¹⁾			Estimated collapse load ⁽²⁾ P (kN)	Experimental collapse load P_{exp} (kN)	$\Delta = \frac{P - P_{exp}}{P_{exp}}$
		LB	DB	GB			
18		×			232.0	-37.1%	
19	18	×		146.0	232.2	-37.1%	
20		×			221.7	-34.1%	

⁽¹⁾ LB-Local Buckling, DB-Distortional Buckling, GB-Global Buckling; ⁽²⁾ See Note 2 to Table 3

Table 5 Results of tests under eccentric load with biaxial bending

ID	Eccentricity e_z (mm)	Buckling mode ⁽¹⁾			Estimated collapse load ⁽²⁾ P (kN)	Experimental collapse load P_{exp} (kN)	$\Delta = \frac{P - P_{exp}}{P_{exp}}$
		LB	DB	GB			
21			×		161.4	-34.2%	
22	$e_y = -14$ mm		×		155.1	-31.5%	
23	$e_z = 36$ mm		×		170.0	-37.5%	
24		×		106.26	173.1	-38.6%	
25	$e_y = 14$ mm	×			175.0	-39.3%	
26	$e_z = 36$ mm	×			169.4	-37.3%	
27		×			168.2	-36.8%	

⁽¹⁾ LB-Local Buckling, DB-Distortional Buckling, GB-Global Buckling; ⁽²⁾ See Note 2 to Table 3

- the buckling mode is distortional for $e_y = -14$ mm and local for $e_y = 14$ mm.

In all tests under eccentric axial load with unsymmetrical bending, specimens loaded with the same eccentricity in both directions exhibited very close values of the collapse load, confirming the reliability of the experimental setup. Depending upon the sign of the eccentricity e_y , specimens exhibited local or distortional buckling.

4. Discussion of experimental results and comparison with code-specified M - N strength domains

In this section, experimental results are compared with M - N strength domains specified in European codes EN 15512 and EN 1993-1-1. Strength domains were built utilizing unitary safety factors and the mean experimental value f_{ym} of the steel yield strength; f_{ym} was evaluated through tensile tests on three steel samples obtained from the same coils of tested column specimens (Fig. 11).

According to EN 15512, the strength domain of elements for which lateral-torsional buckling is a potential buckling mode is defined by the following expression

$$\frac{N_{Ed}}{\chi_{\min} \cdot A_{eff} \cdot \frac{f_y}{\gamma_m}} + \frac{k_{LT} \cdot M_{y,Ed}}{\chi_{LT} \cdot W_{eff,y} \cdot \frac{f_y}{\gamma_m}} + \frac{k_z \cdot M_{z,Ed}}{W_{eff,z} \cdot \frac{f_y}{\gamma_m}} \leq 1 \quad (1)$$

where:

N_{Ed}	design axial load;
$M_{y,Ed}$	design bending moment about y axis;
$M_{z,Ed}$	design bending moment about z axis;
A_{eff}	effective area of the cross-section;
$W_{eff,y}$	effective section modulus about y axis;
$W_{eff,z}$	effective section modulus about z axis;
f_y	steel yield strength;
γ_m	partial safety factor for steel;
χ_{\min} [= min ($\chi_y, \chi_z, \chi_{db}$)]	minimum value among reduction factors due to flexural and distortional buckling;
χ_y, χ_z	reduction factors for flexural buckling;
χ_{LT}	reduction factor for flexural-torsional buckling (CEN 2006b);
χ_{db}	reduction factor for distortional buckling;
k_{LT}	1.0;
k_z	1.5.

Interaction formulas of EN 1993-1-1 for members subjected to combined bending and axial compression are

$$\frac{N_{Ed} \cdot \gamma_{M1}}{\chi_y \cdot A_{eff} \cdot f_{yk}} + k_{yy} \cdot \frac{(M_{y,Ed} + \Delta M_{y,Ed}) \cdot \gamma_{M1}}{\chi_{LT} \cdot W_{eff,y} \cdot f_{yk}} + k_{yz} \cdot \frac{(M_{z,Ed} + \Delta M_{z,Ed}) \cdot \gamma_{M1}}{W_{eff,z} \cdot f_{yk}} \leq 1 \quad (2)$$

$$\frac{N_{Ed} \cdot \gamma_{M1}}{\chi_z \cdot A_{eff} \cdot f_{yk}} + k_{zy} \cdot \frac{(M_{y,Ed} + \Delta M_{y,Ed}) \cdot \gamma_{M1}}{\chi_{LT} \cdot W_{eff,y} \cdot f_{yk}} + k_{zz} \cdot \frac{(M_{z,Ed} + \Delta M_{z,Ed}) \cdot \gamma_{M1}}{W_{eff,z} \cdot f_{yk}} \leq 1 \quad (3)$$

where, in addition to above symbols:

$\Delta M_{y,Ed} = N_{Ed} e_{N,z}$ additional bending moment about y axis due to the shift of the centroidal axis in z direction;

$\Delta M_{z,Ed} = N_{Ed} e_{N,y}$ additional bending moment about z axis due to the shift of the centroidal axis in y direction; [$e_{N,y(z)}$ represents the shift of the centroid of the effective area A_{eff} relative to the center of gravity of the gross cross section, when the cross-section is subjected to compression only; it is evaluated using the method given in EN 1993-1-5 (CEN 2006c)];

$k_{yy}, k_{yz}, k_{zy}, k_{zz}$ interaction factors [the authors utilized the method B (CEN 2006a) for the evaluation of interaction factors k];

γ_{M1}	partial safety factor for steel;
f_{yk}	characteristic yield strength of steel.

Nevertheless, the application of the EN 1993-1-1 formulation to CFS open profiles requires some adaptations, as it is strictly valid only for uniform members with double symmetric cross sections, for sections not susceptible to distortional deformations. Actually, in the first term of both Eqs. (2) and (3) reduction coefficients χ_y and χ_z take into account only flexural buckling, and not torsional buckling, which is typical of unsymmetrical profiles, nor distortional buckling, which is also a potential buckling mode of cold-formed sections. Therefore, the authors introduced in (2) and (3) coefficients χ_y e χ_z suggested in EN 15512, as they are defined as the minimum reduction factors for all possible buckling modes, including flexural-torsional and distortional buckling. Moreover, the additional bending moments $\Delta M_{y,Ed}$ and $\Delta M_{z,Ed}$ were assumed equal to zero,

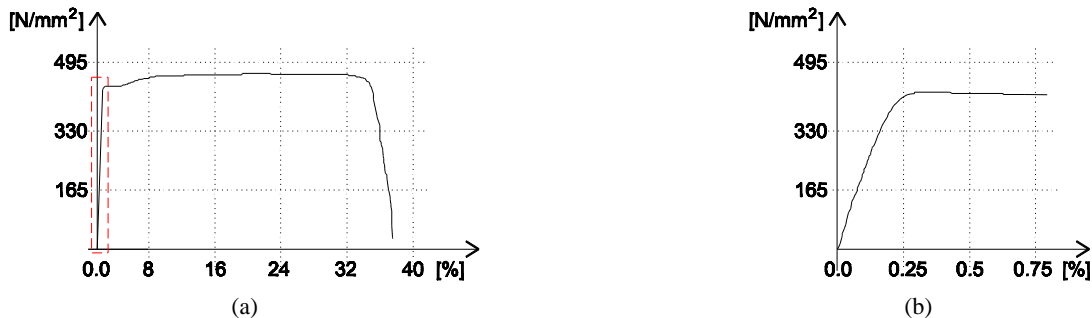


Fig. 11 Tensile test on a steel sample: (a) stress-strain curve; (b) detail of the initial branch

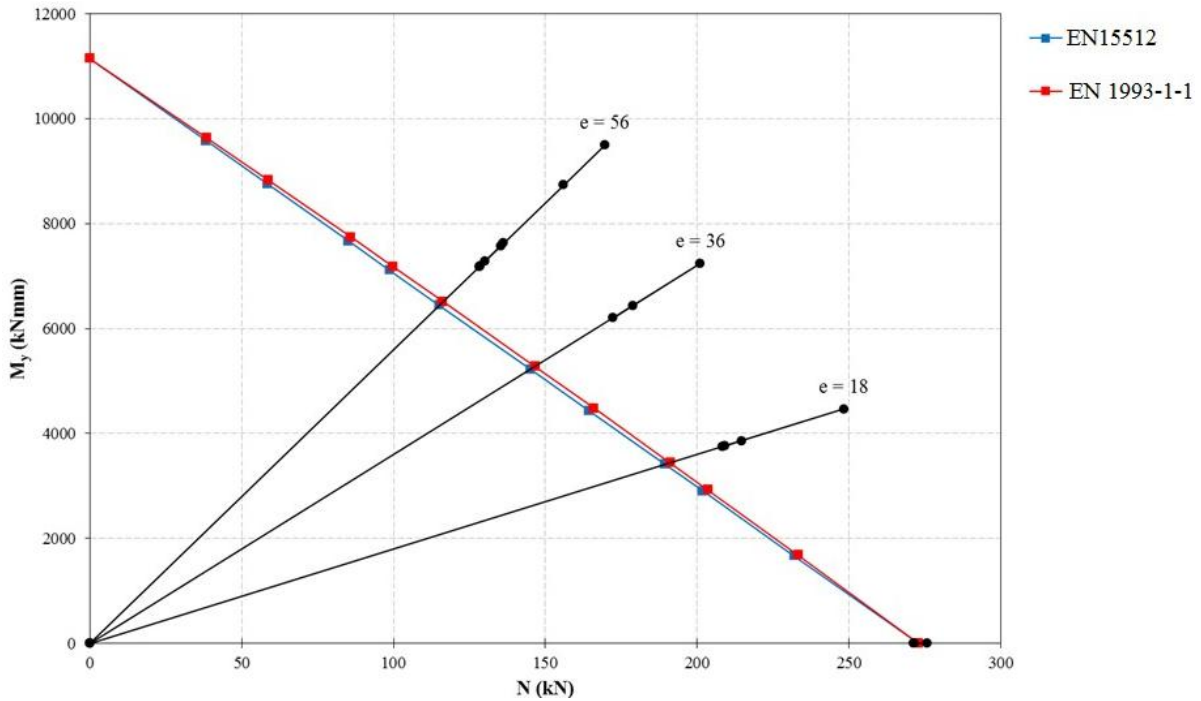


Fig. 12 Strength domain My-N dark points on the lines with constant eccentricity are experimental points

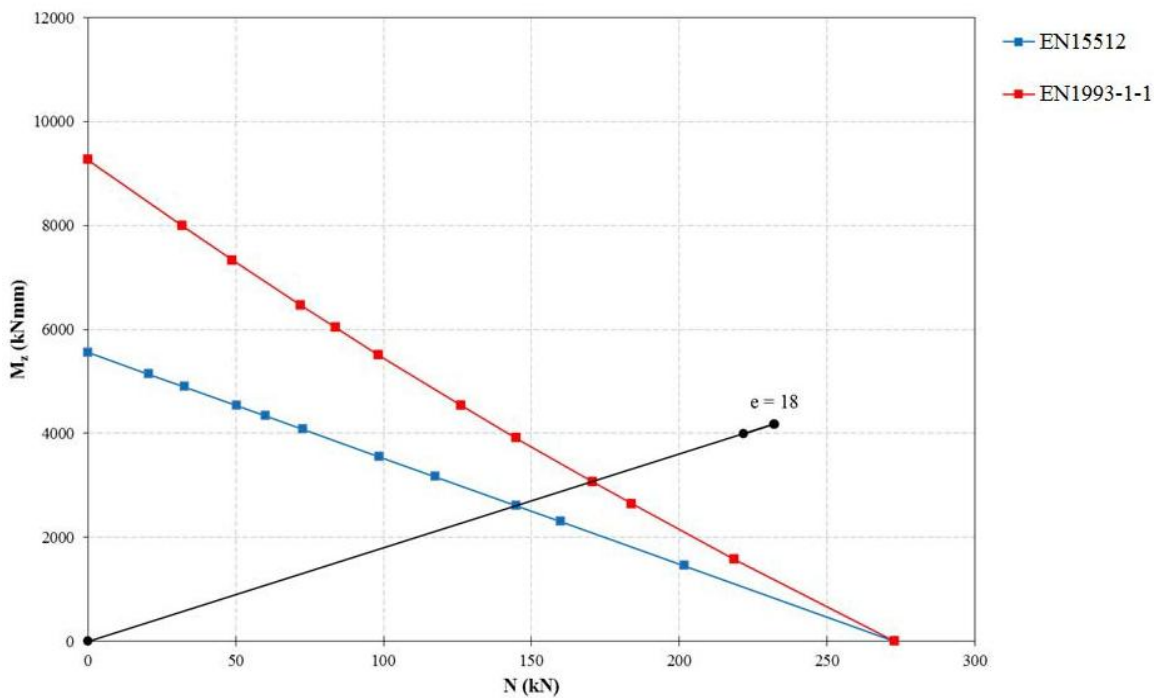


Fig. 13 Strength domain N-Mz: dark points on the lines with constant eccentricity are experimental points

because in the studied open section, the centers of gravity of the gross section and the effective section are almost coincident.

In following paragraphs, theoretical strength domains according to both EN 15512 and EN 1993-1-1 were evaluated and compared with experimental results. To this aim, values of k_{LT} and k_z in Eq. (1) were calculated assuming the equivalent uniform moment factors given by EN 15512 for a triangular shape of the bending moment

diagram. Similarly, values of interaction factors k_{ij} in Eqs. (2) and (3) were taken from Table B.2 of EN 1993-1-1, which holds for members susceptible torsional deformations, using equivalent uniform moment factors C_m given by EN 1993-1-1 for a triangular distribution of bending moments.

Concerning imperfections, they were only measured at midspan of specimens, where an inward closing of flanges was observed and it had about the same value (1÷1.5 mm)

for all specimens. Therefore, an imperfection factor equal to 0.34 was assumed for drawing both domains; this values is suggested in EN 15512 for CFS open sections having a shape similar to the investigated profile.

4.1 M_y - N strength domain

Fig. 12 shows the strength domain M_y - N obtained with both formulations, EN 15512 and adapted EN 1993-1-1. The two formulations give about the same results, as the difference between the two domains, measured along four different lines of constant eccentricity, is about 1.0%. The maximum distance of experimental points from the two strength domains assumes following values:

$\Delta_{EN15512} = 1.0\%$	$\Delta_{EN1993} = 1.0\%$	$e_y = 0 \text{ mm}$	$e_z = 0 \text{ mm}$
$\Delta_{EN15512} = 23.7\%$	$\Delta_{EN1993} = 23.0\%$	$e_y = 0 \text{ mm}$	$e_z = 18 \text{ mm}$
$\Delta_{EN15512} = 27.9\%$	$\Delta_{EN1993} = 27.1\%$	$e_y = 0 \text{ mm}$	$e_z = 36 \text{ mm}$
$\Delta_{EN15512} = 32.1\%$	$\Delta_{EN1993} = 31.4\%$	$e_y = 0 \text{ mm}$	$e_z = 56 \text{ mm}$

For the investigated profile, experimental M_y - N couples at failure are significantly out of these domains, so both codes underestimate ultimate loads.

4.2 M_z - N strength domain

Fig. 13 shows the strength domain M_z - N obtained using both EN 15512 and EN 1993-1-1 formulations. For low axial loads, EN 1993-1-1 gives too much high values of the bending moment about the weak axis z . As the two domains are very close, the maximum distance of experimental points from code domains holds:

$\Delta_{EN15512} = 36.4\%$	$\Delta_{EN1993} = 26.3\%$	$e_y = 18 \text{ mm}$	$e_z = 0 \text{ mm}$
-----------------------------	----------------------------	-----------------------	----------------------

Experimental couples M_z - N are out of both domains and very far from them. Therefore, both formulations are conservative as they neglect a wide region of the strength domain.

4.3 Three-dimensional strength domain

The three-dimensional strength domains according to EN15512 and EN 1993-1-1 have been drawn and compared with experimental results from tests under combined compression and biaxial bending. Each code three-dimensional domain is represented by a plane that passes for three points, which correspond to the ultimate bending moment about the y -axis, the ultimate bending moment about the z -axis and to the ultimate axial load (M_y, R_d, M_z, R_d and N_{Rd}). As tests with biaxial bending were performed for two fixed values of the ratio $M_y/M_z = e_z/e_y$, the corresponding ultimate points are located on the same vertical planes in the space $M_y - M_z - N$, with N -axis in the vertical direction. For $e_y = +18 \text{ mm}$, they are placed on the plane α rotated with respect to z -axis by an angle $+\theta$ (Fig. 10), whose tangent is given by

Fig. 14 shows the three-dimensional domains obtained according to EN 15512 and EN 1993, and the plane α . The intersection between the plane α and each strength domain identifies the frontier M_θ - N of the domain itself on the plane α .

Then in Fig. 15 experimental results are compared with M_θ - N curves. Differently than curves shown in Figs. 12 and 13, in Fig. 15 bending moments were represented on the horizontal axis and axial forces on the vertical axis, so intersection lines AB and AC (Fig. 14) - between the two three-dimensional strength domains and the α plane - can be easily compared.

Maximum differences between experimental points and code-specified strength domains are equal to:

$\Delta_{EN15512} = 38.1\%$	$\Delta_{EN1993} = 30.7\%$	$e_y = 14 \text{ mm}$	$e_z = 36 \text{ mm}$
$\Delta_{EN15512} = 36.3\%$	$\Delta_{EN1993} = 28.7\%$	$e_y = -14 \text{ mm}$	$e_z = 36 \text{ mm}$

5. Conclusions

The response of storage rack uprights with CFS open section has been investigated experimentally through a

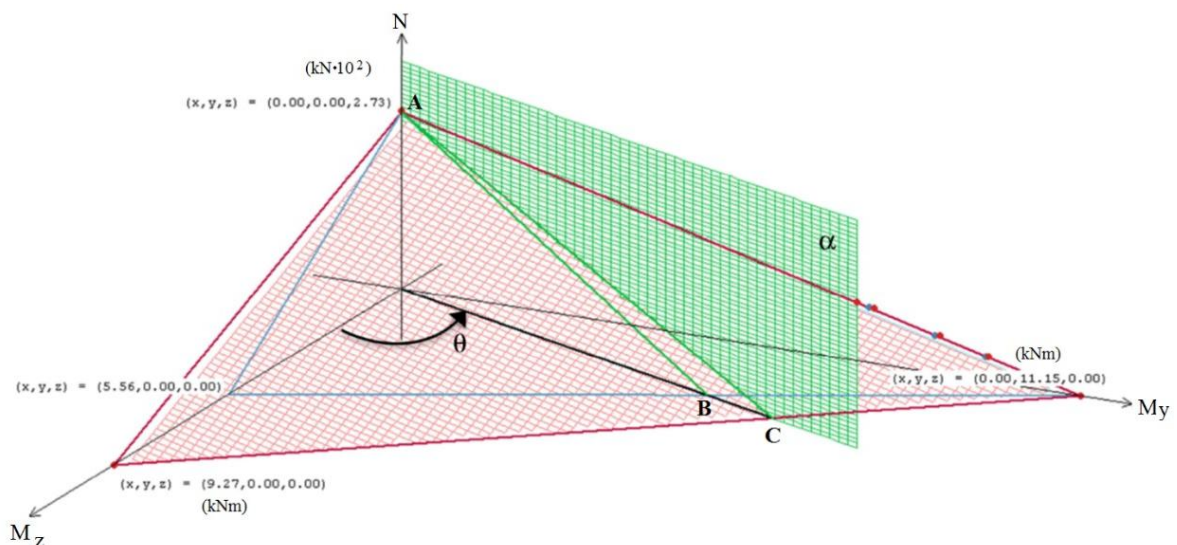


Fig. 14 Three-dimensional strength domains and intersections AB (EN15512) and AC (EN1993-1-1) with α plane

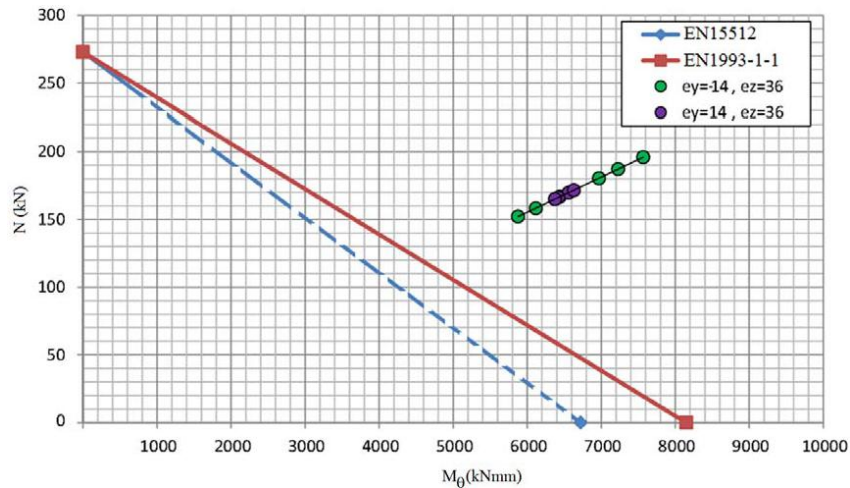


Fig. 15 $N-M_{\theta}$ curves for EN 15512 (dotted line) and EN1993 (continuous line) and experimental points

series of load tests under centric or eccentric axial load. Tests have been conducted preliminarily on stub specimens to assess the geometrical properties of the effective section and then on slender specimens to evaluate the ultimate load and the buckling mode. Pure distortional buckling was observed in a few tests, while the most of slender specimens exhibited a mixed buckling mode. The experimental campaign highlighted that the experimental strength under centric or eccentric axial load of the investigated CFS open profile is much higher than the code-specified strength.

In all tests, the measured collapse load was higher than the predicted one, with the highest differences, up to more than 30%, for specimens under combined axial load and bending about the weak axis z or biaxial bending.

Results suggest deepening the investigation on the behavior of perforated CFS open profiles under combined axial load and bending, with the aim of refining current formulations given in European codes to better fit experimental results for this kind of profiles. To this aim, the authors are already working on the extension of the experimental campaign to other profiles, with different dimensions and/or shape, to check if differences between experimental results and theoretical values are of the same order of magnitude of the present work, and to assess how code provisions could be adapted to better fit the experimental evidence for perforated CFS sections.

The development of the research should give a better approximation of interaction curves of perforated CFS open sections, which could be used to adapt current code-specified formulations to this kind of sections.

Acknowledgments

The authors gratefully acknowledge the Company ROSS S.p.A., Scarperia e San Piero, Florence (Italy), for giving them the possibility of using its laboratory for the execution of the whole experimental campaign, for providing all specimens and for the contribution in planning the research. Particularly, the authors wish to thank Mr. Stefano Bettini (President of the Company) for his active participation, civil engineers Mario Cartacci, Stefano

Lombardi and Francesco Pananti for help in the execution of tests, and building engineers Francesco Socci and Francesco Scavello for help in post-processing of experimental data.

References

- Angotti, F., Galano, L., Orlando, M. and Vignoli, A. (2002), "Assessment of structural performance of HSC slender columns via experimental tests and numerical analysis", *Proceedings of the 6th International Symposium on Utilization of High Strength / High Performance Concrete*, Leipzig, Germany, June; Leipzig University, Institute for Structural Concrete and Building Materials, Volume 1, pp. 149-164. ISBN: 3934178189
- Bernuzzi, C. and Castiglioni, C.A. (2001), "Experimental analysis on the cyclic behaviour of beam-to-column joints in steel storage pallet racks", *Thin-Wall. Struct.*, **39**(10), 841-859.
- Bertocci, L., Comparini, D., Lavacchini, G., Orlando, M., Salvatori, L. and Spinelli, P. (2016), "Experimental, numerical, and regulatory P-Mx-My domains for cold-formed perforated steel uprights of pallet-racks", *Thin-Wall. Struct.* [Submitted]
- Camotim, D., Basaglia, C. and Silvestre, N. (2010), "GBT buckling analysis of thin-walled steel frames: A state-of-the-art report", *Thin-Wall. Struct.*, **48**(10-11), 726-743.
- CEN-COMITÉ EUROPÉEN DE NORMALISATION (2006a), EN 1993-1-1: Eurocode 3: Design of steel structures – Part 1-1: General rules and rules for buildings; Brussels, Switzerland.
- CEN-COMITÉ EUROPÉEN DE NORMALISATION (2006b), EN 1993-1-3: Eurocode 3 - Design of steel structures, Part 1-3: General rules - Supplementary rules for cold-formed members and sheeting; Brussels, Switzerland.
- CEN-COMITÉ EUROPÉEN DE NORMALISATION (2006c), EN 1993-1-5: Eurocode 3 - Design of steel structures. Design of steel structures – Part 1-5: Plated structural elements; Brussels, Switzerland.
- CEN-COMITÉ EUROPÉEN DE NORMALISATION (2009), EN 15512 – Steel static storage systems – Adjustable pallet racking systems – Principles for structural design; Brussels, Switzerland.
- Craveiro, H.D., Rodrigues, J.P.C. and Laím, L. (2016), "Buckling resistance of axially loaded cold-formed steel columns", *Thin-Wall. Struct.*, **106**, 358-375.
- Crisan, A., Ungureanu, V. and Dubina, D. (2012a), "Behaviour of cold-formed steel perforated sections in compression. Part 1 – Experimental investigations", *Thin-Wall. Struct.*, **61**, 86-96.

- Crisan, A., Ungureanu, V. and Dubina, D. (2012b), "Behaviour of cold-formed steel perforated sections in compression. Part 2 – Numerical investigations and design considerations", *Thin-Wall. Struct.*, **61**, 97-105.
- Davies, J.M. (2000), "Recent research advances in cold-formed steel structures", *J. Constr. Steel Res.*, **55**(1), 267-288.
- Davies, J.M., Leach, P. and Taylor, A. (1997), "The design of perforated cold-formed steel sections subject to axial load and bending", *Thin-Wall. Struct.*, **29**(1-4), 141-157.
- Foraboschi, P. (2014), "Experimental characterization of non-linear behavior of monolithic glass", *Int. J. Non-Linear Mech.*, **67**, 352-370.
- Foraboschi, P. (2016), "Versatility of steel in correcting construction deficiencies and in seismic retrofitting of RC buildings", *J. Build. Eng.*, **8**, 107-122.
- Kårman, T.V., Sechler, E.E. and Donnell, L.H. (1932), "The strength of thin plates in compression", *Transact. Appl. Mech. Div., ASME*, **54**(2), 53-57.
- Kesti, J. and Davies, M.J. (1999), "Local and distortional buckling of thin-walled short columns", *Thin-Wall. Struct.*, **34**(2), 115-134.
- Lavacchini, G., Orlando, M., Ortolani, B. and Spadaccini, O. (2013), "Cold-formed steel open profiles: Experimental campaign and comparison with code-specified M-N strength domains", *Costruzioni Metalliche*, **4**, 48-59. [In Italian]
- Lecce, M. and Rasmussen, K. (2006a), "Distortional buckling of cold-formed stainless steel sections: Experimental investigation", *J. Struct. Eng.*, **132**(4), 497-504.
- Lecce, M. and Rasmussen, K. (2006b), "Distortional buckling of cold-formed stainless steel sections: Finite-element modeling and design", *J. Struct. Eng.*, **132**(4), 505-514.
- Li, Z. and Schafer, B.W. (2010), "Application of the finite strip method in cold-formed steel member design", *J. Constr. Steel Res.*, **66**(8-9), 971-980.
- Lian, Y., Uzzaman, A., Lim, J.B.P., Abdelal, G., Nash, D. and Young, B. (2016), "Effect of web holes on web crippling strength of cold-formed steel channel sections under end-one-flange loading condition – Part I: Tests and finite element analysis", *Thin-Wall. Struct.*, **107**, 443-452.
- Moen, C.D. and Schafer, B.W. (2009), "Elastic buckling of thin plates with holes in compression or bending", *Thin-Wall. Struct.*, **47**(12), 1597-1607.
DOI: <http://dx.doi.org/10.1016/j.tws.2009.05.001>
- Papangelis, J.P. and Hancock, G.J. (1995), "Computer analysis of thin-walled structural members", *Comput. Struct.*, **56**(1), 157-176.
- Rondal, J. (2000), "Cold formed steel members and structures: General report", *J. Constr. Steel Res.*, **55**(1), 155-158.
- Salhab, B. and Wang, Y.C. (2008), "Equivalent thickness of cold-formed thin-walled channel sections with perforated webs under compression", *Thin-Wall. Struct.*, **46**(7), 823-838.
- Sarawit, A.T. and Pekoz, T. (2001), "Design of industrial storage racks", *Prog. Struct. Eng. Mater.*, **3**(1), 28-35.
- Schafer, B.W. (2002), "Local, distortional and Euler buckling of thin-walled columns", *J. Struct. Eng.*, **128**(3), 289-299. DOI: [http://dx.doi.org/10.1061/\(ASCE\)0733-9445\(2002\)128:3\(289\)](http://dx.doi.org/10.1061/(ASCE)0733-9445(2002)128:3(289))
- Silvestre, N. and Camotim, D. (2003), "Nonlinear generalized beam theory for cold-formed steel members", *Int. J. Struct. Stabil. Dyn.*, **3**(4), 461-490.
- Sivakumar, K.S. and Abdel-Rahman, N. (1998), "A finite element analysis model for the behaviour of cold-formed steel members", *Thin-Wall. Struct.*, **31**(4), 305-324.
- StruMetaL (2015), *Strutture Metalliche Leggere per Magazzini Autoportanti ad Elevata Capacità (Light Steel Structures for Self-Supporting Warehouses with Large Storage Capacity)*; Research Program partially supported by Tuscany Region (Regional Operational Programme CreO FESR 2007-2013, Lines of Action 1.5.a and 1.6, Call for Proposals R&D 2012, D.R. 189/2012 - prot. N. 19044).
- Szabo, I.F. and Dubina, D. (2004), "Recent research advances on ECBL approach. Part II: Interactive buckling of perforated sections", *Thin-Wall. Struct.*, **42**(2), 195-210.
- Teh, L.H., Hancock, G.J. and Clarke, M.J. (2004), "Analysis and design of double-sided high-rise steel pallet rack frames", *J. Struct. Eng.*, **130**(7), 1011-1021.
- Ungureanu, V., Madeo, A., Zagari, G., Zucco, G., Dubina, D. and Zinno, R. (2016), "Koiter asymptotic analysis of thin-walled cold-formed steel uprights pallet racks structures", *Structures*, **8**, 286-299.
- Yan, J. and Young, B. (2002), "Column tests of cold-formed steel channels with complex stiffeners", *J. Struct. Eng.*, **128**(6), 737-745.
- Young, B. and Chen, J. (2008), "Column tests of cold-formed steel non-symmetric lipped angle sections", *J. Constr. Steel Res.*, **64**(7), 808-815.
- Young, B. and Rasmussen, J.R. (1998), "Tests of fixed-ended plain channel columns", *J. Struct. Eng.*, **124**(2), 131-139.
- Zagari, G., Zucco, G., Madeo, A., Ungureanu, V., Zinno, R. and Dubina, D. (2016), "Evaluation of the erosion of critical buckling load of cold-formed steel members in compression based on Koiter asymptotic analysis", *Thin-Wall. Struct.*, **108**, 193-204.

CC